

# 10D.7 THE ROLE OF INTERACTIONS BETWEEN MULTI-SCALE CIRCULATIONS ON THE OBSERVED ZONALLY AVERAGED ZONAL WIND VARIABILITY ASSOCIATED WITH THE MADDEN-JULIAN OSCILLATION

Naoko Sakaeda\* and Paul Roundy

Department of Atmospheric and Environmental Sciences

University at Albany, State University of New York, Albany, NY 12222, U.S.A

## 1. INTRODUCTION

The Madden-Julian Oscillation (MJO; Zhang 2005) is a dominant mode of intraseasonal variability in tropical convection and circulation. Numerous observational studies have documented that the anomalous tropical convection associated with the MJO influences the global circulation in multiple time and space scales. Several studies have shown that the MJO interacts with some extratropical teleconnection patterns such as the Arctic Oscillation, the North Atlantic Oscillation and the Pacific North American patterns (Cassou 2008; Lin et al. 2009; Mori and Watanabe 2008). Others have shown that the MJO modulates the propagation characteristics of high frequency extratropical transient eddies (Matthews and Kiladis 1999), characteristics and frequency of breaking Rossby waves (Moore et al. 2010), as well as violent tornado outbreak frequency in the North America (Thompson and Roundy 2013). These interactions might actively influence the evolution of the MJO itself, therefore further studies of the interaction between the MJO and the extratropics could improve understanding of MJO dynamics and long-range forecast skill in global circulation.

In order to understand the interactions between the MJO and the extratropical circulation that involve multi-scale interactions from a simplified point of view, this study examines the less explored association between the zonal mean intraseasonal circulation and the MJO. The study focuses on the 200hPa level where the zonally averaged climatological subtropical jets maximize in their amplitude during the boreal winter. The jets act as waveguides of extratropical Rossby waves and as storm tracks. Therefore the emphasis on the association between the variability in the subtropical jets and the MJO is important for understanding of consequential influences of the transient eddies and synoptic weather events such as wave breaking and blocking. This study diagnoses the role of zonal mean and eddy circulation and their multi-scale interactions on the upper-level zonal mean zonal wind variability associated with the MJO through budget analysis.

## 2. DATA and MJO Indices

Wind data is obtained from Global National Center for Environmental Prediction Climate Forecast System

Reanalysis data (Saha et al. 2010) with 2.5 degree horizontal resolution on isobaric surfaces. Interpolated Outgoing Longwave Radiation (OLR, Liebmann et al. 1996) data obtained from NOAA Earth System Research Laboratory is applied as a proxy for moist deep convection in the tropics. The period of the study is December-January-February (DJF) from 1980 to 2010.

The MJO indices used here are calculated as by MacRitchie and Roundy (2012) except the intraseasonal timescale is defined as 20-100 days and only the OLR component is projected to generated the indices. These indices are similar to Real-time Multivariate MJO indices of Wheeler and Hendon (2004), but are derived using filtered OLR and wind data.

## 3. METHODOLOGY

### 3.1 Empirical Orthogonal Function (EOF) Analysis

EOF analysis is applied to 20-100 day filtered zonally averaged 200hPa zonal wind data during DJF to extract its dominant modes of intraseasonal variability. The difference in grid box density with latitude is taken into account by multiplying by the cosine of latitude before the EOF analysis is applied. The first two leading EOFs of the zonal wind, shown in Figure 1, explain around 33% and 21% of the variance. The first EOF shows oscillation of the intraseasonal zonal wind in the tropics. The second EOF shows meridional shifts of the Northern and Southern Hemisphere subtropical jets that occur symmetrically about the equator. The principal components of the first and the two leading EOFs are referred to as PC1 and PC2 respectively.

Figure 2 shows that the average period of PC1 is

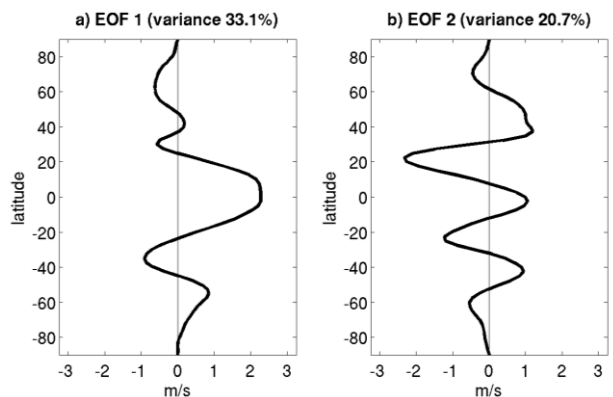


FIG 1: First two leading EOFs of the zonally-averaged intraseasonal zonal wind at 200hPa with amplitude for one standard deviation of each PC.

\*Corresponding author address: Naoko Sakaeda, Univ. at Albany, Dept. of Atmospheric and Environmental Sciences, Albany, NY, 12222; email: nsakaeda@albany.edu

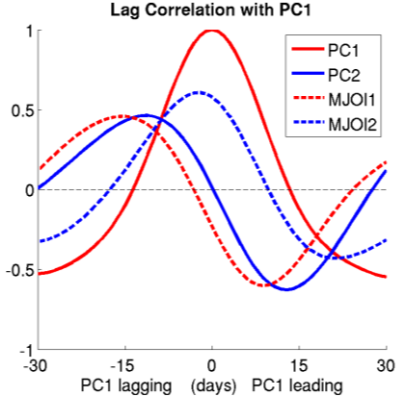


FIG 2: Auto-correlation of PC1 and its cross-correlations with PC2 and MJO indices.

about 54 days and PC1 and PC2 are most correlated with each other at about  $\pm 13$ -days time lag with the correlations of about  $-0.62$  and  $0.46$ . The correlation is higher when PC1 leads PC2, suggesting that the equatorial intraseasonal signal tends to precede the subtropical meridional shifts while the tropical wind signal following the anomalous meridional shift of the subtropical jets may vary more in the periodicity and amplitude.

PC1 and PC2 are also highly correlated with the MJO indices with some time lags (Fig. 2 only showing PC1). Correlation between the PC1 or PC2 and MJO indices exceeding 0.6 indicates the first two leading EOFs of the zonally averaged intraseasonal zonal wind are closely coupled to the convective part of MJO that is captured by the MJO indices. The correlation between the MJO indices and higher number PCs drops to around or less than 0.2, indicating less coupling between MJO convection and higher EOFs of the zonal wind.

### 3.2 Zonally-averaged Zonal Momentum Equation

The dynamical mechanisms that drive the intraseasonal zonal wind are examined through budget analysis on zonal momentum equations with linear time decompositions. When zonally averaged, zonal momentum equations simplify into

$$\frac{\partial [u]}{\partial t} = -[v] \frac{\partial [u]}{\partial y} - [\omega] \frac{\partial [u]}{\partial p} - \frac{\partial}{\partial y} [\{u\}\{v\}] - \frac{\partial}{\partial p} [\{u\}\{\omega\}] + f[v] + [X] \quad (1)$$

(Holton 2004), where the square brackets represent the zonal mean and the curly bracket represents deviation from zonal mean.  $X$  represents the sum of other terms deemed negligible in the broader circulation away from the most intense organized deep convection. The results presented in this extended abstract focus on the first and the third dynamical terms on the right hand side (rhs) of (1) that are referred to: meridional advection by zonal mean winds (term1) and meridional eddy flux convergence (term3).

In order to study the role of interactions across timescale, wind data are decomposed into three-frequency bands including –the intraseasonal time scale

defined by 20-100 days, and periods longer and shorter than that scale. The longer and shorter timescales are referred to as the background state and transient scale. The background state includes the seasonal cycle and other low frequency climate signals such as the El Niño/Southern Oscillation (ENSO) or climate change. The seasonal cycle is defined as the annual cycle and its first three harmonics. The data are filtered by applying the Fourier transform, setting coefficients outside of the selected bands to zero, and performing the inverse transform. Although this approach can result in Gibbs ringing, the bands are broad, and our tests reveal that ringing has little impact on results. All the derivatives are calculated using 5 points centered differentiation. The background, intraseasonal, and transient timescales are represented by the over bar, star and prime respectively as shown below for both zonal mean and eddy winds in (2) and (3).

$$[u] = [\bar{u}] + [u^*] + [u'] \quad (2)$$

$$\{u\} = \{\bar{u}\} + \{u^*\} + \{u'\} \quad (3)$$

The time decomposition into three timescales results in further expansion of the first four terms on the rhs of (1) into 9 terms each. It results in terms that involve interaction between different timescales. Each calculated term is then filtered for the intraseasonal band to assess its contributions to signals in that band as indicated by stars outside the terms in (4) and (5). For zonal mean advection terms (term1 and term2), the scale analysis showed that the only terms that contribute to the intraseasonal timescale are the terms that represent interaction between the background and intraseasonal band as shown in (4) for term1.

$$\left( -[v] \frac{\partial [u]}{\partial y} \right)^* \approx -[v] \frac{\partial [u^*]}{\partial y} - [v^*] \frac{\partial [\bar{u}]}{\partial y} \quad (4)$$

$$(\text{Term1})^* \approx (\text{Term1a-1})^* + (\text{Term1a-2})^*$$

These terms are considered pseudo-linear since the background state can be considered constant within the intraseasonal timescale. Whereas for the convergence of eddy flux terms (term3 and term4), nonlinear momentum transfer from transient eddies plays an important role as well (5).

$$\left( -\frac{\partial}{\partial y} [\{u\}\{v\}] \right)^* \approx \left( -\frac{\partial}{\partial y} [\{u^*\}\{\bar{v}\}] - \frac{\partial}{\partial y} [\{\bar{u}\}\{v^*\}] \right)^* + \left( -\frac{\partial}{\partial y} [\{u'\}\{v'\}] \right)^* \quad (5)$$

$$(\text{Term3})^* \approx \underbrace{(\text{Term3a-1} + \text{Term3a-2})^*}_{(\text{Term3a})^*} + (\text{Term3b})^*$$

The role of these four terms, term1a-1, term1a-2, term3a and term3b for driving the 200hPa zonal mean intraseasonal zonal wind are examined and discussed in Section 4.

### 3.3 Lagged Regression Techniques

The association between the zonal mean zonal wind and the MJO is examined based on the dominant spatial structure of intraseasonal zonal wind variability extracted by EOF analysis shown in Section 3.1. In order to capture the evolving wind tendency, driving mechanism, and MJO convection associated with the EOF patterns, lagged regression is used with the PCs as predictors. The gridded fields are regressed against the normalized PCs with time lags. The fields are then reconstructed using the regression coefficients and one standard deviation of the predictor PC. Statistical significance is tested at each grid point by using the correlation coefficient.

## 4. RESULTS

Because PC1 and PC2 are highly correlated given a time lag, the results presented here will focus on evolution and mechanism associated with the development of the EOF1 pattern only. The repeated analysis using PC2 suggests similar mechanisms to that suggested by analysis of EOF1.

### 4.1 Evolution of the Zonal Mean Circulation with the MJO

Figure 3b shows the evolution of intraseasonal zonal wind and its time tendency, as linearly associated with PC1 using the regression technique described in Section 3.3. The intraseasonal zonal wind anomaly starts over the tropics and propagates poleward as its amplitude weakens. The wind signal is stronger in the Northern Hemisphere (NH) and there is an equatorward propagating wind anomaly from higher latitudes that has the opposite sign of wind anomaly that propagates from the tropics. A similar equatorward propagating signal does not occur in the Southern Hemisphere (SH), where the wind signal from the tropics propagates to higher latitudes than in the NH. The DJF climatological zonal mean jets peak at around 30°N and 50°S (Fig. 3a). When the opposite sign intraseasonal zonal wind anomalies approach the latitudes of jet peaks, it results in a few degree latitudinal shift of the jets long with a change in amplitude of a few  $\text{m s}^{-1}$ .

This zonal mean intraseasonal zonal wind is signal highly associated with a zonally asymmetric signal in MJO convection. Figure 4 maps the longitudinal structures of the intraseasonal zonal wind and MJO convection at days -15, -5, +5, and +15. The envelope of enhanced MJO convection is over the Maritime continent to the western Pacific basin when the zonal mean intraseasonal wind begins to become anomalously westerly (Fig. 4a). At the same time, the poleward shift of the subtropical jets is indicated by the anomalous westerly and easterly wind poleward and equatorward of the climatological location of the jet streams respectively. As the MJO active convection propagates to the central Pacific basin, the tropical intraseasonal zonal wind anomaly reaches its maximum westerly state (Fig. 4b). A suppressed convective envelope of the MJO develops over the Indian Ocean as the zonal mean intraseasonal westerly wind

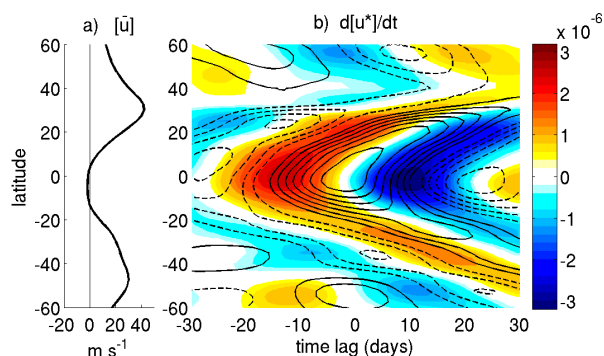


FIG. 3: (a) Composite of DJF zonal mean background zonal wind. (b) Time-latitude diagram of intraseasonal zonal wind tendency (shaded,  $\text{m s}^{-2}$ ) and intraseasonal zonal wind (black contour with  $0.3 \text{ m s}^{-1}$  interval) obtained by lag regression onto one standard deviation of PC1. Only the values with statistical significance with 95% confidence level are shaded.

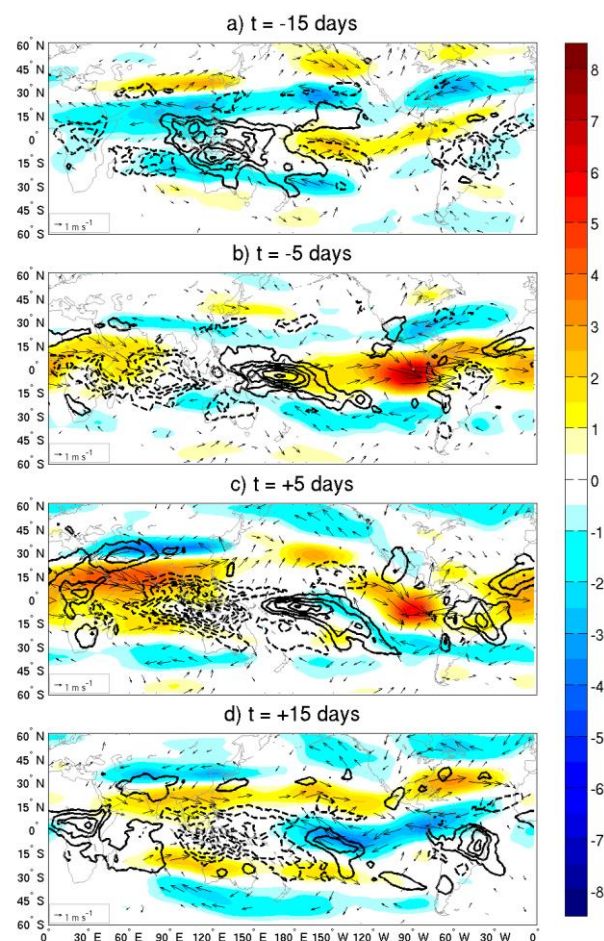


FIG 4: Lag regression map of intraseasonal zonal wind (shaded,  $\text{m s}^{-1}$ ) and intraseasonal OLR anomalies (black solid and dashed indicate negative and positive values respectively, at  $2 \text{ W m}^{-2}$  interval) onto one standard deviation of PC1. At time lags of -15 days (a), -5 days (b), +5 days (c), and +15 days (d).

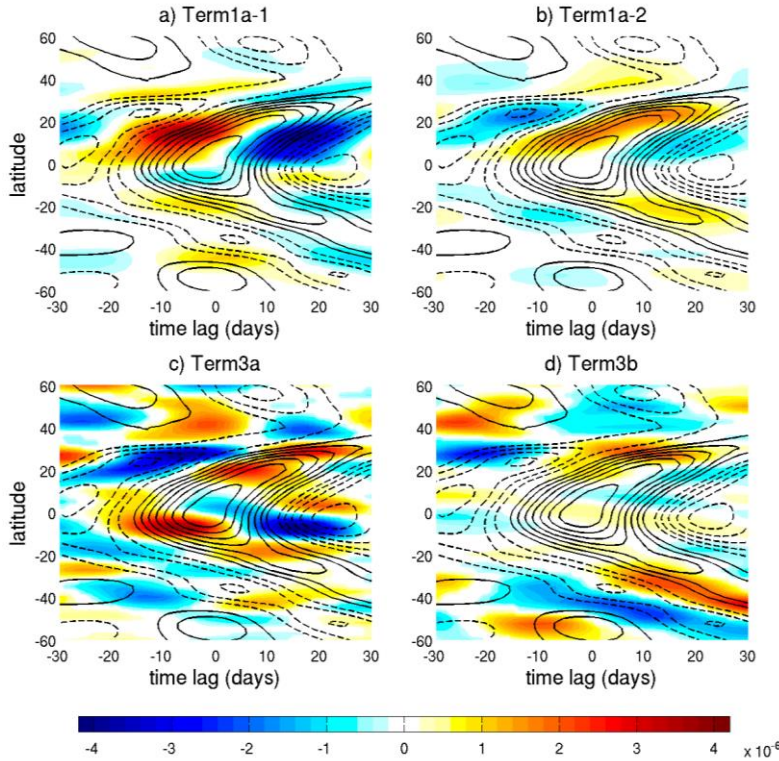


FIG. 5: Same as Fig. 3 except shaded are term1a-1 (a), term1a-2 (b), term3a (c), and term 3b (d) in unit of  $\text{m s}^{-2}$ .

propagates poleward (Fig. 4c). The subtropical jets shift equatorward with the decay of the tropical westerly wind anomaly, followed by the anomalous zonal mean tropical zonal wind switching to easterly as the suppressed convective phase of the MJO moves to the central Pacific (Fig. 4d). The anomalous upper-tropospheric zonal mean intraseasonal zonal winds are also coupled to the zonal mean meridional overturning circulation that expands throughout the troposphere (not shown).

#### 4.2 Key Driving Mechanisms I: Interactions of Background and Intraseasonal Zonal Mean Flows

This section examines the contribution to the intraseasonal zonal wind by the dynamical process that involves interactions of background and intraseasonal zonal mean winds, term1a.

Figure 5 shows the intraseasonal zonal wind acceleration by the advection of intraseasonal wind by the background wind, term1a-1 ( $-\bar{v}[\partial u^*/\partial y]$ , Fig.5a), and the advection of background state by intraseasonal wind, term1a-2 ( $-[v^*](\partial \bar{u}/\partial y)$ , Fig. 5b). The strong northward propagation of the intraseasonal zonal wind over the northern subtropics is driven by term1a-1, suggested by term1a-1 leading the zonal wind signal in quadrature. The seasonal zonal mean meridional wind is southerly from  $20^\circ\text{S}$  to  $30^\circ\text{N}$  with its amplitude maximizing around  $10^\circ\text{N}$  (not shown). Therefore induced zonal mean intraseasonal wind in the tropics is

advected northward and the advection is stronger in the NH. This result suggests that the structure of the climatological seasonal mean circulation plays a key role in driving the observed northward propagation of the intraseasonal zonal wind.

Term1a-2 contributes more at higher latitudes as the meridional shear of the background zonal wind is stronger around the subtropical jet. This advection by the intraseasonal wind (term1a-2) is more in phase with the zonal wind, indicating that it acts to maintain the intraseasonal zonal wind rather than to propagate it. It results from propagation of the zonal mean intraseasonal meridional wind  $[v^*]$  that is in phase with the zonal wind  $[u^*]$ .

The examination of the zonal mean advection terms shows that the evolution of the zonal mean intraseasonal wind is partly determined by how it is advected by the background flow rather than how it advects the background flow. It indicates that the changes in the background state would have strong influence on the zonal mean circulation associated with the MJO. However, the zonal mean advection terms alone

cannot explain the change in the equatorial intraseasonal zonal wind anomaly and why the anomaly is able to extend poleward of  $20^\circ\text{N}$  or  $20^\circ\text{S}$ .

#### 4.3 Key Driving Mechanism II: Interaction between Background and Intraseasonal Eddies

The important contributions to the changes in the tropical intraseasonal zonal wind come from term3a ( $-\partial[\bar{u}]\{v^*\} + \{u^*\}\{\bar{v}\}/\partial y$ , Fig.5c), especially between the equator and  $15^\circ\text{S}$ . Term3a can be interpreted as anomalous meridional flux convergence resulting from modulation of the background eddy circulation due to intraseasonal eddies. The climatological DJF mean meridional flux convergence by background eddies accelerates westerly wind in the SH tropics and easterly wind in the NH and SH subtropics (Fig.6a left panel). Convection in the tropics is also climatologically most active over the western Pacific warmpool region (Fig.6a), which plays a role in forming the climatological eddy circulation patterns.

When term3a accelerates westerly wind over the SH tropics around day -15, the envelope of enhanced MJO convection coincides with where the convection is active in climatological mean (Fig. 4a). On this day, the intraseasonal eddy circulation generally coincides with the background eddies (Fig. 6b). This combination results in strengthening of the background eddies and the flux convergence, resulting in anomalous westerly acceleration over the SH tropics and easterly acceleration over the NH subtropics. At day +15, when MJO convection suppresses the background convection

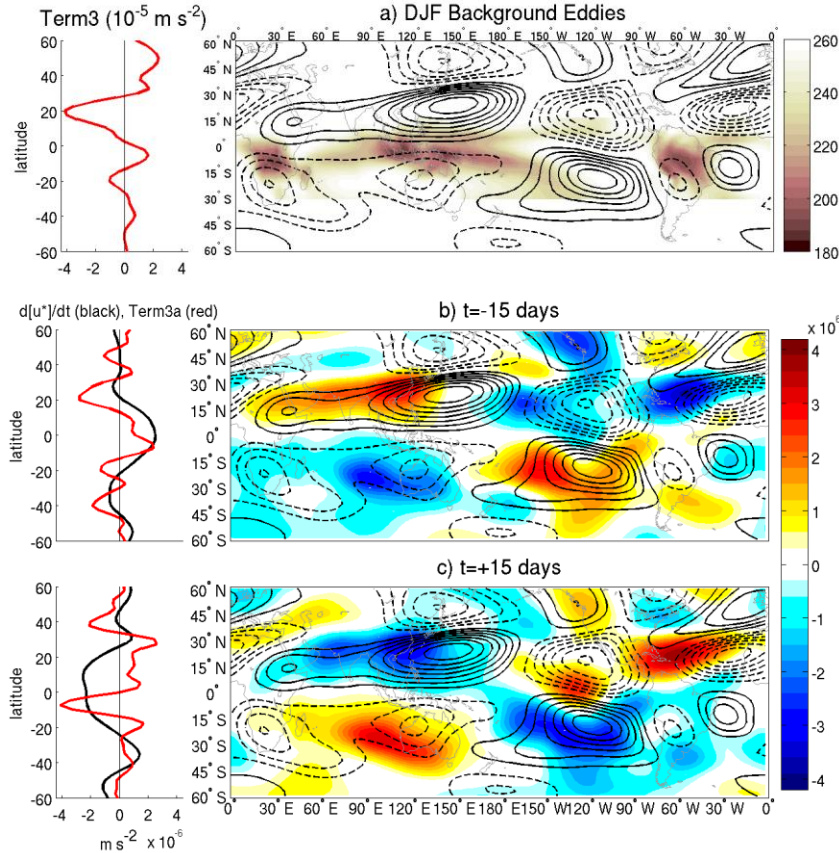


FIG. 6: (a) Meridional profile of DJF mean term3 on left and composites of DJF OLR (shaded,  $\text{Wm}^{-2}$ ) and 200hPa background eddy streamfunction (plotted with  $4 \times 10^6 \text{ m}^2 \text{ s}^{-1}$  interval, black solid and dashed represent positive and negative values). (b,c) intraseasonal zonal mean zonal wind tendency (black) and term3a (red) on left panels and 200hPa intraseasonal eddy streamfunction is shaded on maps. Black contour represent is the same composites of background eddy streamfunction as (a). Plotted for day -15 (b) and +15 (c).

over the warmpool (Fig. 4d), intraseasonal circulation acts to weaken the background eddies (Fig. 6c). Therefore the flux convergence by the modulated background eddies over the SH tropics weakens and induces anomalous easterly acceleration.

#### 4.4 Key Driving Mechanism III: Flux Convergence by Transient Eddies

Fig. 5d shows that the further poleward propagation of the intraseasonal zonal wind pattern poleward of 20°N and 20°S is contributed by term3b. Term3b represents feedback onto the intraseasonal zonal wind from the changes in the characteristics of the transient eddies including meridional shift of their tracks and changes in the south-to-north tilt of their trough/ridge axes.

The structural and track changes in the transient eddies at day -15 and day +5 are evidenced in Figure 7 by first identifying the days of local peaks in PC1 with amplitude greater than one standard deviation. Then the days during which transient eddy meridional wind at

30°N and 150°W were southerly 15 days prior and 5 days after the peaks in PC1 are composited. The composite 200hPa transient eddy streamfunction (shaded in Fig.7) is compared with its climatological structure (contoured in black in Fig. 7) which is composited based on all days when the transient eddy meridional wind at the same location was southerly during DJF. Statistical significance for these composites is tested by 1000 sample bootstrap resampling tests as described by Roundy et al. (2010). The distribution of the 1000 times resampled composite days are compared with 1000 composites based on sets of the same number of dates selected at random from DJF. At each grid point, if the distribution of the resampled composite is greater or smaller than 95% of the distribution based on the random composite, the results is deemed statistically significant.

Fig. 7a shows that the transient eddies tend to be more positively tilted with latitude (anticyclonically sheared) at day -15. While at day +5, they are more south-north oriented and their track has shifted slightly southward compared to their climatological structure. On these time lags, the MJO circulation response imposes planetary scale intraseasonal anticyclonic (-15 days) and cyclonic (+5 days) shear on the

subtropical jet in the NH (Fig. 4a and 4c). These anomalous intraseasonal shear patterns influence the baroclinic lifecycle of the synoptic eddies as anti-cyclonic (LC1) and cyclonic (LC2) Rossby wave breaking tends to occur in background anticyclonic and cyclonic shear, respectively (Thorncroft et al. 1993). Similar changes occur over the central North Pacific and North Atlantic basins as well (not shown). These modulated structures of the synoptic eddies change the meridional profile of  $\{u\}\{v\}$  (Figure 8a) that induces its anomalous meridional convergence and accelerates intraseasonal easterly wind at -15 days and westerly wind at +5 days to the south of climatological jet around 30°N (Fig. 8b). Along with other mechanisms, this positive feedback develops midlatitude intraseasonal zonal wind variability associated with the MJO.

## 5. CONCLUSION

The results help explain the driving mechanisms of the observed global circulation patterns associated with the MJO that have not been explained previously.

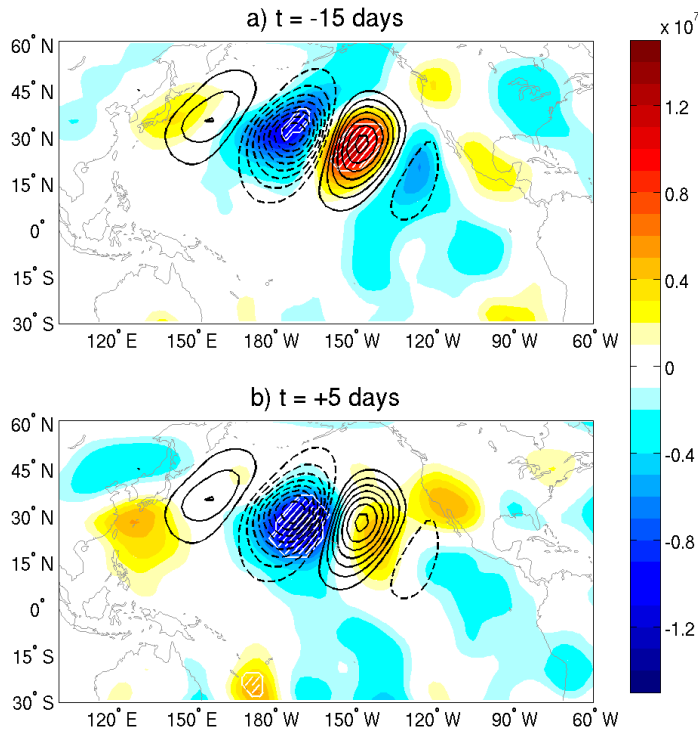


FIG 7: Composite maps of 200hPa transient eddy streamfunction at (a) -15 day and (b) +5 day from the peak of PC1 with greater than 1 standard deviation (see text for more details). The transient eddy streamfunction ( $\text{m}^2 \text{s}^{-1}$ ) is shaded and its climatological composite is contoured in black with  $10^6 \text{m}^2 \text{s}^{-1}$  interval (N=20 days for (a) and 17 days for (b)). Hatched region indicate statistical significance with 95% confidence level using bootstrap re-sampling test for shaded anomalies.

Three key mechanisms drive the northward propagation of the intraseasonal zonal wind in the NH. The first is the advection of intraseasonal zonal wind by the background zonal mean meridional wind. The second is the changes in the background eddy circulation by intraseasonal eddies to induce anomalous momentum flux convergence. The third is that the intraseasonal circulation modulates the behaviors of the transient eddies, which then feed back onto the intraseasonal zonal mean zonal wind.

These results reveal that scale interactions drive the intraseasonal circulation. The results also suggest that interactions of intraseasonal circulations with the background state and consequential changes in the synoptic eddies can change the subsequent MJO circulation structure leading to its event-to-event variability.

## 6. REFERENCES

- Cassou, C., 2008: Intraseasonal interaction between the Madden-Julian oscillation and the North Atlantic oscillation. *Nature*, **455**, 523-527.
- Holton, J. R., 2004: The zonally averaged circulation. *An introduction to dynamic meteorology*, F. Cynar, Ed., Elsevier Academic Press, 316-328.

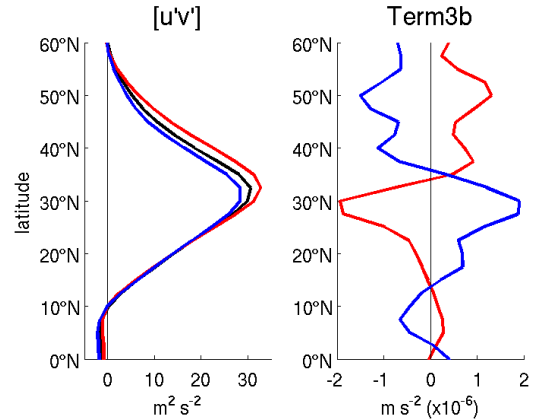


FIG 8: Meridional profiles of (a) total  $[\{u'\}\{v'\}]$  and (b) term3b obtained by lag regression onto one standard deviation of PC1. Profiles on day -15 are shown in red and day +5 in blue. Black profile in (a) shows DJF climatological profile of  $[\{u'\}\{v'\}]$ .

Liebmann, B., and C. A. Smith, 1996:

Description of a complete (interpolated) outgoing longwave radiation dataset. *Bull. Amer. Meteor. Soc.*, **77**, 1275-1277.

Lin, H. L., G. Brunet, and J. Derome, 2009: An observed connection between the North Atlantic Oscillation and the Madden-Julian Oscillation. *J. Climate*, **22**, 364-380.

MacRitchie, K. and P. E. Roundy, 2012:

Potential vorticity accumulation following atmospheric Kelvin waves in the active region of the MJO. *J. Atmos. Sci.*, **69**, 908-914.

Matthews, A. J. and G. N. Kiladis, 1999: The tropical-extratropical interaction between high-frequency transients and the Madden-Julian oscillation. *Mon. Wea. Rev.*, **127**, 661-677.

Mori, M. and M. Watanabe, 2008: The growth and triggering mechanisms of the PNA: a MJO-PNA coherence. *J. Meteor. Soc. Japan*, **86**, 213-236.

Roundy, P. E., C. J. Schreck, and M. A. Janiga, 2009: Contribution of convectively coupled equatorial Rossby waves and Kelvin waves to the real-time multivariate MJO indices. *Mon. Wea. Rev.*, **137**, 469-478.

Saha, Suranjana, and Coauthors, 2010: The NCEP climate forecast system reanalysis. *Bull. Amer. Meteor. Soc.*, **91**, 1015-1057.

Thompson, D. B. and P. E. Roundy, 2013: The relationship between the Madden-Julian oscillation and U.S. violent tornado outbreaks in the spring. *Mon. Wea. Rev.*, **141**, 2087-2095.

Thorncroft, C. D., B. J. Hoskins, and M. E. McIntyre, 1993: Two paradigms of baroclinic-wave life-cycle behavior. *Q. J. R. Meteor. Soc.*, **119**, 17-55.

Zhang, C., 2005: Madden-Julian Oscillation. *Rev. Geophys.*, **43**, RG2003, doi:10.1029/2004RG000158